JOURNAL OF MATERIALS SCIENCES 26 (1991) 4186–4193

The microstructure and mechanical properties of Bi(Pb)-Sr-Ca-Cu-Ag metallic precursor ribbons produced by the melt-spinning process

WEI GAO, SONG-CHUN LI, R. PARRELLA, D. A. RUDMAN, J. B. VANDER SANDE
Department of Materials Science and Engineering, Massachusetts Institute of Technology, Cambridge, MA 02139, USA

Metallic precursor ribbons of Bi-Pb-Sr-Ca-Cu with nominal compositions of 1.4-0.6-2-3-4, respectively, were made by vacuum induction melting followed by melt-spinning. Silver at the level of 12–81 vol% was added to produce precursor-Ag alloy ribbons. These ribbons were subjected to a controlled atmosphere oxidation and annealing to produce superconducting oxide/Ag microcomposites. All of the alloys with up to 73 vol% Ag can be processed into superconducting ribbons with zero resistance at $T = 104$–110 K and a critical current density of 200–600 A cm^{-2} at 77 K in zero field. The relationship of the Ag content, melt-spinning processes, microstructure and mechanical properties of the metallic precursor ribbons were studied by microhardness tests, bending tests, scanning electron microscopy and electron probe microanalysis. The maximum bending strain of the metallic precursor ribbons was found to increase from 0.3–1.7% as the silver content increased from 12–81 vol%, while the ribbon hardness was found first to increase with silver content increasing from 12–62 vol%, then to decrease with further increases in silver content. The mechanical properties were also strongly affected by the melt-spinning processes, *i.e.* by the ejection pressure applied to the melt and wheel surface speed. The best bending strain for the metallic precursors with 52 vol% Ag achieved so far is ~0.85%, which was obtained by using an ejection pressure of 69 kPa and a wheel speed of 9.5 m s^{-1}. The mechanical properties of the precursor ribbons is critically important for producing superconducting coils and long wires, which were made by first winding the metallic ribbons on MgO spools, followed by suitable oxidation and annealing.

1. Introduction

Among various methods to produce high T_c superconducting oxides, one method is high temperature oxidation of metallic precursor alloys that contain the metallic constituents of the superconducting oxides [1–5]. Noble metals (e.g. Ag) have been added to those metallic precursors to yield superconducting oxide/noble metal microcomposites in order to improve their mechanical properties. This method can be used to produce high T_c superconducting wires as well as coils. Superconducting coils or long wires can be made by first winding the metallic ribbons on MgO spools, followed by suitable oxidation and annealing. Therefore, the mechanical properties of the precursor ribbons are important for manufacturing superconducting coils and wires. We have been performing research involving high temperature oxidation of Bi(Pb)-Sr-Ca-Cu-Ag metallic precursors to produce superconducting oxide/Ag microcomposites. Bi-Pb-Sr-Ca-Cu-Ag metallic precursor ribbons and coatings were produced by melt-spinning and melt-dipping, and then converted to superconducting oxides by oxidation at a relatively low temperature in an oxidizing atmosphere followed by an annealing at a relatively high temperature. Superconducting oxide/Ag microcomposites with zero resistance at $T = 104$–110 K and critical current density of ~ 600 A cm^{-2} at 77 K in zero field were produced in this way with excellent reproducibility [5–8]. In the present paper, we discuss the effect of the silver content and melt-spinning processing parameters on the microstructures and mechanical properties of the metallic precursor ribbons.

2. Experimental procedure

Ten alloys were investigated in the present work. Their nominal composition (atomic proportions) is Bi 1.4–Pb 0.6–Sr 2–Ca 3–Cu 4, with 3, 5, 8, 11, 14, 21, 36, 42, 52 and 82 Ag, respectively, which correspond to 25–90 wt% or 12–81 vol% Ag. The nominal alloy compositions are listed in Table I, together with the volume percentages of silver in the alloys. The volume percentages of silver were first calculated by using the average densities of all the elements involved, then calibrated by using measured alloy densities. The alloy numbers A3–A82 refer to the nominal atomic proportions of Ag in the alloy, and are used to represent

0022–2461/91 $03.00 + .12

these alloys throughout this work. Alloy A21 (with 52 vol % Ag) has been transformed into superconducting microcomposites with the highest critical current density (500–700 A cm^{-2}) among all of the alloys, and it was chosen to study the effect of the melt-spinning processing parameters. To eliminate the potential effect of composition variation, a single ingot was used to study the effect of melt-spinning processing parameters, specifically alloy A21.

The metallic precursor ribbons were produced by first mixing and melting the pure metals together, then remelting and spinning into metallic ribbons. The melting chamber was evacuated at room temperature to a pressure of 10^{-4} torr before heating. All of the pure metals ($\geqslant 99.9\%$) were put into a tantalum crucible, which does not react with the liquid alloys. Pure Ar at 1.3 atm pressure was introduced into the vacuum chamber when heated to 500 °C. The alloys were fully melted at about 1200 °C and allowed to cool slowly in the Ta crucible. The alloy ingots were then sectioned with a diamond wafering saw with mineral oil as the lubricant.

Approximately 10 g pieces of these alloys were melted again quickly under 0.3 atm Ar pressure in a fused silica crucible, and the liquid alloy was ejected by applying an Ar gas over pressure. The liquid alloy was ejected through a nozzle in the bottom of the crucible onto a rotating copper wheel with a well polished surface.

Several processing parameters are thought to be important for the mechanical properties of the melt-spun ribbons, they are: 1. the temperature of the melt during ejection; 2. the size of the nozzle; 3. the distance from the nozzle to the wheel surface; 4. the gas pressure applied to eject the melt on to the wheel surface; and 5. the wheel surface speed. Among these factors, the applied ejection pressure and wheel speed have shown the most significant effects and were relatively easy to control. In the first part of the experiments (to study the effect of the silver content), the temperature of the melt before ejection was about 1250 °C, the diameter of the nozzle was 0.8 ± 0.1 mm, the gap between the nozzle and wheel surface was 2 ± 0.2 mm, the surface speed of the wheel was ~ 8 m s^{-1} and the ejection pressure was ~ 28 kPa. In the second part of the experiment (to study the effect of the melt-spinning processes), the wheel surface speed varied from 6.3 to 19.2 m s^{-1} and the applied ejection pressure varied from 14 to 97 kPa, the temperature of the melt (~ 1250 °C), the size of the nozzle (0.8 ± 0.1 mm) and the gap between the nozzle and the wheel surface (2 ± 0.2 mm) were kept constant. These processes yielded continuous metallic precursor ribbons of 40–100 μm in thickness, 2–3 mm wide and up to 5 m in length. These ribbons were handled in ambient atmosphere, and can be stored in glass bottles in an Ar atmosphere for at least 6 months without losing their metallic luster and mechanical properties.

The metallic precursor ribbons were mounted in resin to prepare cross-section metallographic specimens with standard mechanical polishing. Microhardness tests were performed in a LECO DM-400 Hardness Tester on these same specimens using a load of 25 g to obtain Vickers hardness H_v. Ten points were measured for each specimen. To calculate the results, two of the largest and two of the smallest measurements were deleted and the remaining "middle six" were used to determine the average value of H_v.

The bending tests were performed by fitting straight ribbons on round glass tubes with different diameters. These ribbons showed elastic bending and pure brittle fracture when the silver content was low. When the silver content was high, the ribbons showed a mixed brittle and ductile fracture as some residual deformation can be seen after bending and after breaking. The radius of the smallest tube on which the ribbon can be fitted entirely without breaking was taken as the maximum bending radius R. The maximum surface engineering bending strain ε was used to characterize the bending properties of these ribbons, and calculated by using [9]:

$$\varepsilon = t/2R$$

where t is the thickness of the ribbon. Again ten measurements were performed for each alloy, and the averages of the "middle six" were used to represent the bending behaviour.

Microstructural observation and microanalysis were performed in a JEOL Superprobe 733 Microanalyzer with Tracor Northern 5500–5600 WDS and EDS systems. Backscattered electron images (BSE) were used to show both microstructure and microcomposition of the specimens because it exhibits different contrast from the different phases consisting of different elements. Pure metals of Bi, Cu and Ag, $CaCO_3$, $SrCO_3$ and $PbSiO_4$ were used as the standards for quantitative analysis.

3. Results and discussion

3.1. Effect of the silver content

The measured Vickers hardness, H_v, and maximum bending strain, ε, of the precursor ribbons with different silver content are listed in Table I, together with the volume percentage of silver in the alloys. Fig. 1 shows the plots of H_v against Ag vol % and ε against Ag vol %. It can be seen that the Vickers hardness, H_v, of the precursor ribbons increased from ~ 100 to 280 as the silver content increased from 12 to 62 vol %, then decreased from 280 to 200 as silver increased further to 81 vol %, exhibiting a peak of ~ 280 around 60 % Ag. Different hardnesses were observed near the chilled surface (wheel surface) and free surface of the melt-spun ribbons. The chilled surface has a higher hardness than the free surface, especially for those alloys with $\geqslant 33$ vol % Ag. For instance, the hardness near the chilled surface was 10–20 % higher than near the free surface in alloys A42–A82, and 5–15 % higher in alloys A11–A36, indicating that microstructures with a smaller grain size (obtained near the chilled surface due to the higher cooling rate) possess higher hardness.

On the other hand, the maximum bending strain of the precursor ribbons ε increased continuously as the silver content increased from 12 to 81 vol %. At first ε increased slowly from ~ 0.3 to 0.7 % as the silver

TABLE I Nominal compositions, microhardness and maximum bending strain of the metallic precursor ribbons used in the study. Alloy number refers to the nominal atomic proportion of Ag.

Alloy no.	Nominal atomic proportion Bi	Pb	Sr	Ca	Cu	Ag	Vol % Ag	Micro-hardness H_v (± 20)	Maximum bending strain ε, ± 0.1%
A3	1.4	0.6	2	3	4	3	12	108	0.30
A5	1.4	0.6	2	3	4	5	18	155	0.42
A8	1.4	0.6	2	3	4	8	26	173	0.48
A11	1.4	0.6	2	3	4	11	33	189	0.55
A14	1.4	0.6	2	3	4	14	40	257	0.60
A21	1.4	0.6	2	3	4	21	52	269	0.65
A36	1.4	0.6	2	3	4	36	62	275	0.70
A42	1.4	0.6	2	3	4	52	68	246	1.0
A52	1.4	0.6	2	3	4	52	73	231	1.4
A82	1.4	0.6	2	3	4	82	81	202	1.7

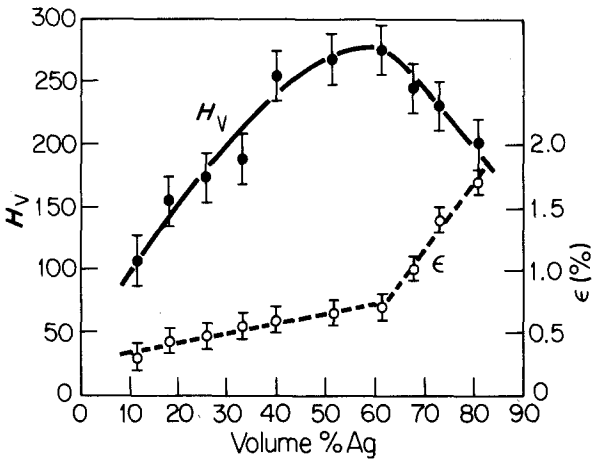

Figure 1 Microhardness and maximum bending strain against the silver content. The Vickers hardness, H_v's, were obtained by using 25 g load; the maximum bending strain, ε, was obtained by dividing one-half of the ribbon thickness with the maximum bending radius; the silver content was expressed with the Ag volume percentage in the alloy.

content increased from 12 to 62 vol %, then went up much faster from 0.7 to 1.7% as the silver content increased from 62 to 81 vol %. ε = 0.7–1.7% correspond to minimum winding diameters $2R$ = 14–6 mm with a ribbon thickness of 50 μm. The maximum bending strains were slightly greater when the chilled surface faced outwards than inwards, indicating that the material near the chilled surface has better strength and toughness than near the free surface. This also suggested that the mechanical properties of the precursor ribbons can be further improved by increasing the cooling rate.

Fig. 2 is a set of SEM backscattered electron (BSE) micrographs, showing the cross section microstructure from alloys A3, A5, A11, A21, A36 and A52. This is a very complicated alloy system consisting of six elements. Phase diagrams [10–13] showed that these six elements can be divided into two groups, Bi, Pb, Cu and Ag in the first group and Ca and Sr in the second. The elements from the first group react with the elements in the second to form intermetallic compounds, some of which have high melting points ~ 1200 °C, e.g. Ca_3Bi_2 and Ca_2Pb. This is why the alloys did not melt until about 1200 °C. The elements in the same group are shown to be entirely miscible (Ca-Sr and Cu-Pb), or to form eutectic phases (Ag-Cu, Ag-Pb, Bi-Pb and Bi-Ag). However, no phase diagram is available for the complete system.

As shown in Fig. 2, these alloys have a fine scale, multiphase crystalline structure, as one can expect from a complicated system consisting of many phases. Because of the high cooling rate, the grain sizes are small, and the phases distributed rather homogeneously. Microanalysis with an electron beam diameter of 10 μm showed little difference throughout the entire cross section. The upper sides in all the micrographs correspond to the chilled surface (wheel surface) where the structure was finer than in the center and near the free surface. The average grain sizes were estimated as 2, 1 and 0.8 μm for alloys A3, A5 and A11, showing that the grain size became smaller as the silver content increased. While the alloy A3 showed a microstructure containing Ag-rich grains 2–6 μm long, 1–2 μm wide (Fig. 2a), alloys A11, A21, A36 and A52 exhibit structures with Ca-, Cu- and Sr-rich dark grains distributed in the Ag-rich matrix. The size of those dark grains was similar for alloys A11–A52, mostly between 0.5–1.0 μm, and their amount decreased with the increase of silver, as shown in Fig. 2c–f.

The effect of the silver content on the mechanical behaviour described above can be explained as the result of several factors. Firstly, the different phases have different hardness and strength. The Ca(Sr)- and Cu-rich phases (dark areas in BSE images) have a smaller average hardness than silver rich phases, as we observed in the hardness measurements. Therefore, when the volume percentage of the Ca(Sr)- and Cu-rich phases were high, the average hardness of the alloy was low and increased with silver, as observed in alloys A3–A36. On the other hand, when the silver content was high, the Ca(Sr)- and Cu-rich phases can be effective as hardening phases in the silver rich phase, so that the alloy hardness was high and decreased with silver, as we observed in alloys A36–A82. These two effects resulted in the peak in the H_v against Ag % plot where the hardening effect of the Ca(Sr)- and Cu-rich phases in the silver rich phase reached the maximum, as shown in Fig. 1.

The maximum bending behaviour is more complicated, because it is a function of strength (hardness),

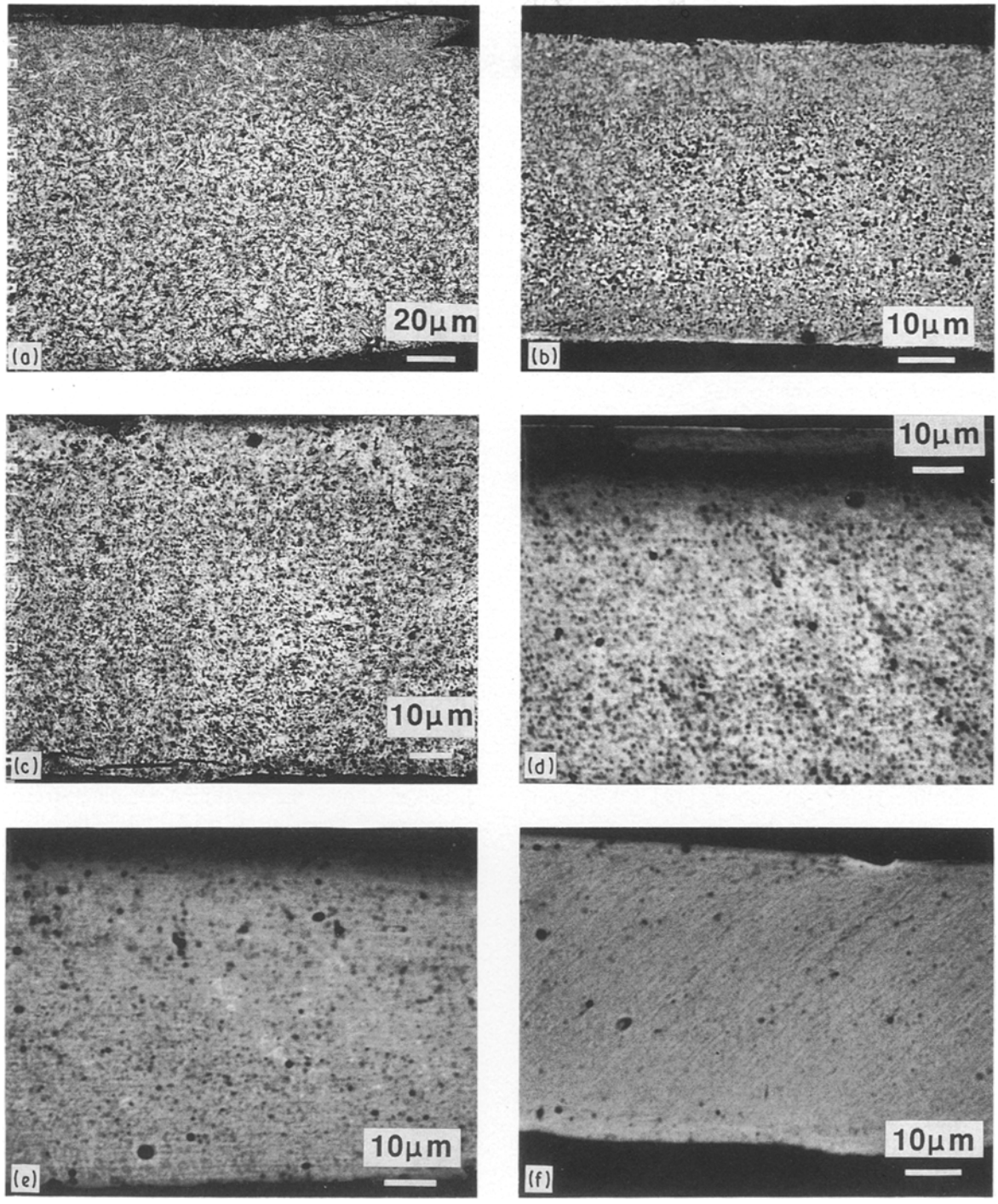

Figure 2 Scanning electron micrographs (backscattered electron images) of the cross section microstructure from metallic precursor ribbons of $Bi_{1.4}Pb_{0.6}Sr_2Cu_3Cu_4$- with (a) Ag_3, (b) Ag_5, (c) Ag_{11}, (d) Ag_{21}, (e) Ag_{36} and (f) Ag_{52}.

toughness (ductility) and perfection of the ribbons, and highly defect sensitive. As shown in Fig. 1, the maximum bending strain increased slowly with the alloy hardness (strength) as the silver content increased from 12 to ~ 62 vol % (A3–A36), then increased much faster when the alloy showed increasing ductility as the silver content increased from 62–81 vol % (A36–A82). This also agreed with the microstructural observation shown in Fig. 2, that the grain size became smaller as the silver content increased from 12–33 vol %, which contributed to the maximum bending strength and toughness, and the amount of second phases decreased as the silver content further increased from 52–82 vol %, which improved the ductility of the specimens.

3.2. Effect of the melt-spinning parameters

The effects of the ejection pressure, P, and wheel surface speed, v, on the microhardness, H_v, and maximum bending strain, ε, of the melt-spun ribbons for alloy A21 are listed in Table II, together with the ribbon thickness, t. While P varied from 14 to 97 kPa and v varied from 6.3 to 19.2 m s^{-1}, the temperature of the melt, the size of the nozzle and the gap between the nozzle and the wheel surface were kept constant. Fig. 3 shows the plots of H_v against P and ε against P, Fig. 4 shows the plots H_v against v and ε against v, all for alloy A21. As shown from the plots, H_v decreased from ~ 320 to ~ 230 as the pressure increased from 14 to 97 kPa. This is expected since as the ejection pressure increased, the amount of the melt ejected onto the

TABLE II The effects of the ejection pressure, P, and wheel surface speed, v, on the microhardness, H_v, and maximum bending strain, ε, of the melt-spun ribbons of alloy A21, together with the ribbon thickness, t. The temperature of the melt = ~ 1250 °C, the size of the nozzle = 0.8 ± 0.1 mm and the gap between the nozzle and the wheel surface = 2 ± 0.2 mm.

$H_v/\varepsilon(\%)/t(\mu m)$	Ejection pressure (kPa)			
Wheel speed ($m\,s^{-1}$)	14	28	69	97
6.3		244/0.43/88		
9.5	320/0.57/43	277/0.67/58	235/0.85/64	230/0.52/102
14.8		227/0.54/48		
19.2		224/0.32/40		

wheel surface rotating with a constant speed increased. This caused the thickness of the ribbons to increase, and therefore the cooling rate and hardness of the melt-spun ribbons to decrease, as shown in Fig. 3 and Table II. On the other hand, under a constant ejection pressure $P = 28$ kPa, H_v first increased from ~ 244 to ~ 277 as the wheel speed increased from 6.3 to 9.5 $m\,s^{-1}$, then decreased to about ~ 224 as the wheel speed further increased to 19.2 m, exhibiting a maximum hardness of H_v = ~ 277 around $v = 9.5\,m\,s^{-1}$, as shown in Fig. 4.

There are a number of references discussing the models for formation of metallic ribbons in the so-called chill block melt-spinning (CBMS) process [14–17]. Cooling rate is often used to characterize rapid solidification processes, although the high growth rate in rapid solidification processes can also be a result of a large undercooling [14]. Cooling rate in the CBMS process depends on a number of factors, including the nature of the melt and substrate material, the time and distance over which the ribbon remains in contact with substrate, etc. In this experiment, the contact time decreased with the increase in the wheel speed. This can be used to explain the hardness of the ribbon decreasing from H_v = ~ 277 to ~ 226 as the wheel speed decreased from 9.5 to 19.2 $m\,s^{-1}$. However, further decreases in the wheel speed from 9.5 to 6.3 $m\,s^{-1}$ produced much thicker melt-spun ribbons (88 μm), and therefore caused the ribbon hardness to decrease, as shown in Fig. 4.

The plots of the maximum bending strain ε against the applied pressure P and the wheel surface speed v exhibit peaks of ε = ~ 0.67% at v = ~ 9.5 $m\,s^{-1}$ when $P = 28$ kPa and ε = ~ 0.85 at $P = 69$ kPa when $v = 9.5\,m\,s^{-1}$, as shown in Figs 3 and 4. As discussed above, the maximum bending strain is a complicated mechanical behaviour. The ε–v plot shows a similar tendency as the H_v–v plot, as shown in Fig. 4, indicating that good strength (hardness) resulted in a good bending strain. This suggested that ε was affected predominantly by the ribbon strength. The ε–P plot, however, did not follow the same tendency as the H_v–P plot, implying that a more complicated mechanism was involved. The ribbons obtained with $P = 69$ kPa showed the highest maximum bending strain (0.85%) and some ductile deformation during bending, suggesting that under this ejection pressure, the ribbons possess a combination of good strength and some ductility. On the other hand, although the lower ejection pressures ($P = 14$ and 28 kPa) produced ribbons with higher hardness (Fig. 3), the ribbon surfaces were often rough and the

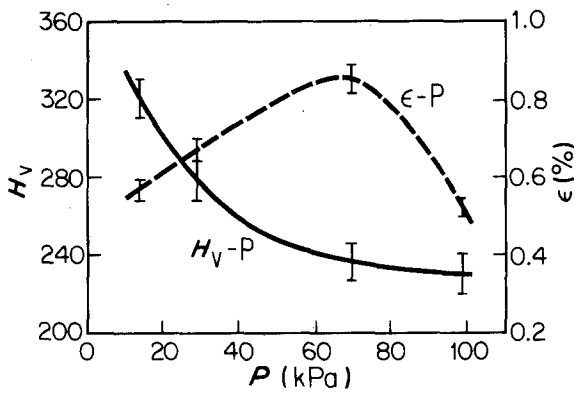

Figure 3 Hardness, H_v, and maximum bending strain, ε, against applied ejection pressure P for alloy $Bi_{1.4}Pb_{0.6}Sr_2Cu_3Cu_4Ag_{21}$; the wheel speed, v, was 9.5 $m\,s^{-1}$.

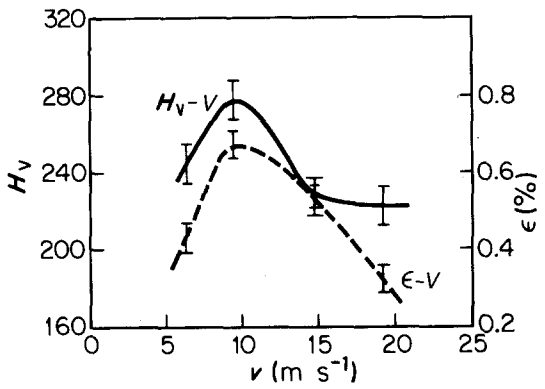

Figure 4 Hardness, H_v, and maximum bending strain, ε, against wheel speed, v, for alloy $Bi_{1.4}Pb_{0.6}Sr_2Cu_3Cu_4Ag_{21}$; the applied ejection pressure, P, was 28 kPa.

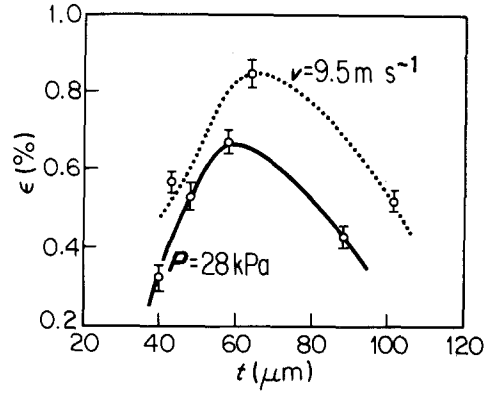

Figure 5 Maximum bending strain, ε, against ribbon thickness, t, for alloy $Bi_{1.4}Pb_{0.6}Sr_2Cu_3Cu_4Ag_{21}$. The same data from Figs 3 and 4.

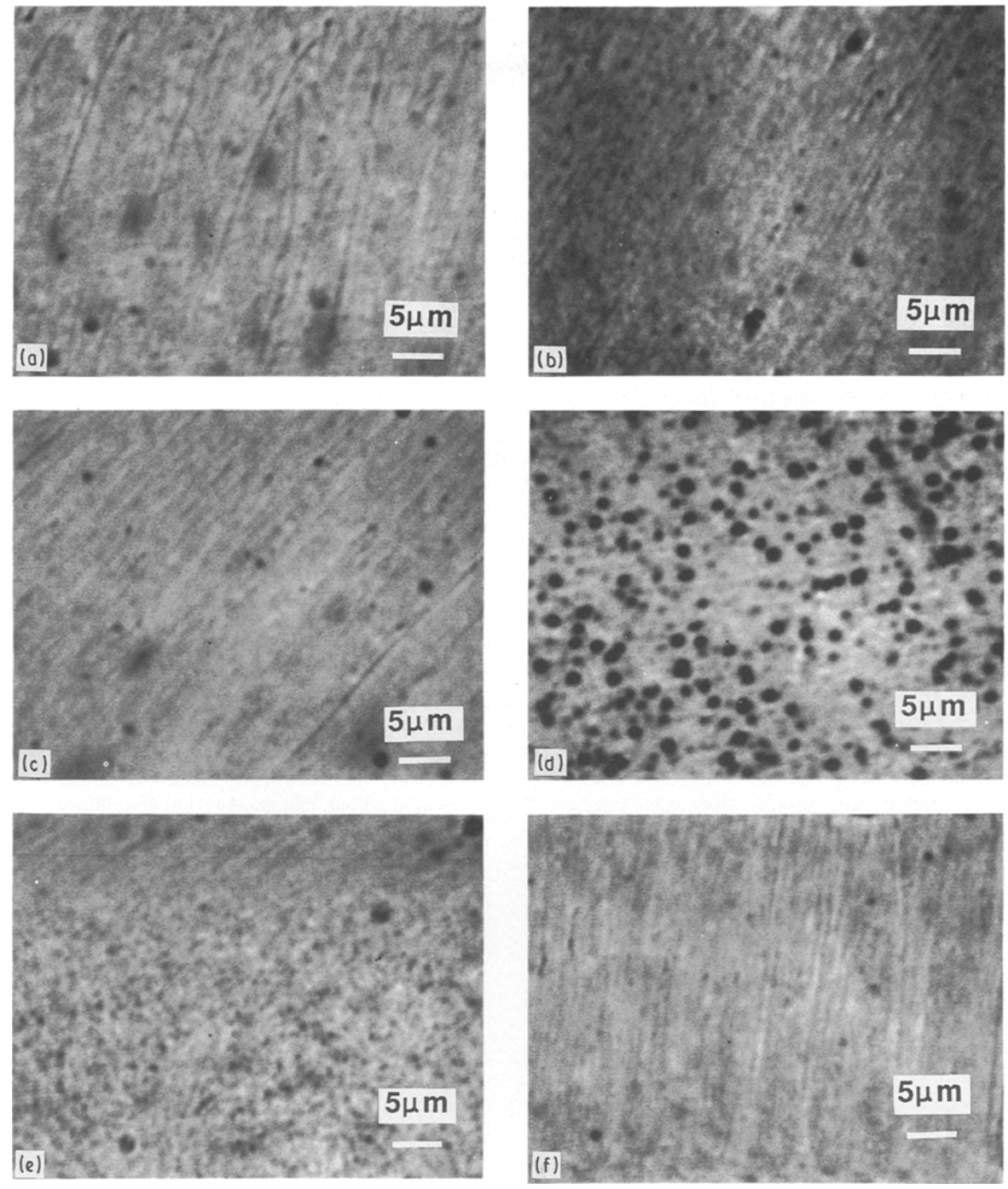

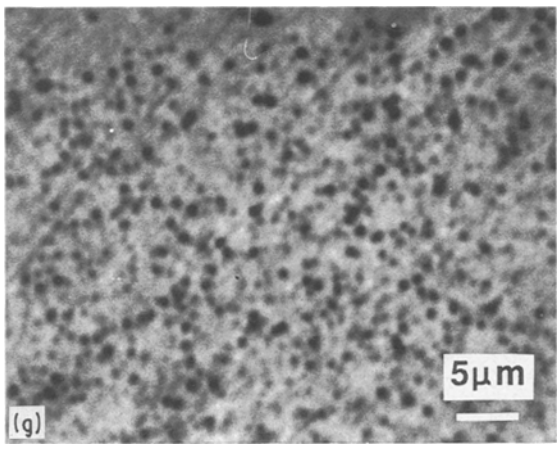

Figure 6 Scanning electron micrographs (backscattered electron images) of typical cross section microstructure from $Bi_{1.4}Pb_{0.6}Sr_2Cu_3Cu_4Ag_{21}$ produced with different melt-spinning parameters: (a) ejection pressure $P = 14$ kPa, wheel speed $v = 9.5\,m\,s^{-1}$, (b) $P = 28$ kPa and $v = 9.5\,m\,s^{-1}$, (c) $P = 69$ kPa and $v = 9.5\,m\,s^{-1}$, (d) $P = 97$ kPa and $v = 9.5\,m\,s^{-1}$, (e) $P = 28$ kPa and $v = 6.3\,m\,s^{-1}$, (f) $P = 28$ kPa and $v = 14.8\,m\,s^{-1}$, (g) $P = 28$ kPa and $v = 19.2\,m\,s^{-1}$.

ribbon quality was poor, which contributed to decreasing their maximum bending strain. Fig. 5 shows two plots of ε against the ribbon thickness t, corresponding respectively to the ε–P and ε–v plots in Figs 3 and 4. It can be seen that the best bending properties obtained were from the ribbons with thickness around 60 μm. This also can be generally explained as follows: When the ribbons were too thick (> 80 μm), the cooling rate was low and the ribbon strength and maximum bending strain became low; when the ribbons were too thin (< 50 μm), the quality of the ribbon surface was poor as were the bending properties.

Fig. 6 is a set of SEM (BSE) micrographs, showing the cross section microstructure from alloy A21 produced with different melt-spinning processing parameters. Fig. 6a to d correspond to those produced with a constant wheel speed of 9.5 $m\,s^{-1}$ and ejection pressures of 14, 28, 69 and 97 kPa, respectively. Fig. 6e, f and g are micrographs produced with a constant ejection pressure of 28 kPa and wheel speeds of 6.3, 14.8 and 19.2 $m\,s^{-1}$, respectively. Two different features were found in these microstructures: Fig. 6d, e and g showed many dark grains of a second phase while the remainder showed very few dark grains. It is believed that the segregation of this dark phase was related to the cooling rate during the melt-spinning. Segregation took place when the ejection pressure was high (Fig. 6d), or the wheel speed was high (Fig. 6g), or the wheel speed was so low that it produced thick ribbons (Fig. 6e). Even in Fig. 6e and g, segregation did not appear near the wheel surface where the cooling rate was higher than in the middle. The microstructural observations agreed with the ribbon mechanical properties, as the maximum bending strain decreased with the existence of this phase segregation. However, no attempt was made to give a quantitative analysis to the bending behaviour of these metallic precursor ribbons because of its complicated nature.

The other processing parameters also influenced the ribbon mechanical properties. For instance, the nozzle size affected the thickness and width of the resulting ribbons. When the nozzle size was too small (< 0.6 mm), the ribbon hardness was relatively high but the ribbon quality was poor as were the bending properties; when the nozzle size was too large (> 1.2 mm), the resulting ribbons were thick and wide, the ribbon hardness and strength became smaller, and the ribbon quality also became difficult to control. The temperature of the melt affected the ribbon quality in a similar way to the ejection pressure: lower temperature resulted in a thinner ribbon and higher hardness. Again if the temperature was too high or too low, the processing and the ribbon quality were difficult to control. On the other hand, the gap between the nozzle and wheel surface were found to be relatively unimportant in establishing the ribbon properties. Little difference in ribbon hardness and bending properties can be detected with the gap size varying from 1 to 3 mm.

As reported in our previous papers [6, 18], all the precursor alloys with up to 73 vol % Ag can be converted into superconducting microcomposite ribbons with $T_{R=0} = 104$–110 K and $J_c = 200$–600 $A\,cm^{-2}$ at 77 K in zero field by suitable oxidation and annealing treatments. Fig. 7 is the SEM (BSE) micrographs showing typical longitudinal cross section microstructures from specimens of A5 and A21 oxidized at 600 °C in 100% O_2 for 40 h, followed by annealing at 835 and 820 °C in 5% O_2 + 95% Ar for 100 h. Silver grains (marked A) show bright contrast and the superconducting oxide $(Bi, Pb)_2Sr_2Ca_2Cu_3O_x$ (the so-called "2223" phase) exhibits grey contrast (marked B). Superconducting coils with diameters as small as 8–10 mm have been produced using the following procedure: metallic precursor ribbons were first wound on MgO spools, which do not react with the superconducting phases at elevated temperatures, then converted to superconducting coils by suitable oxidation and annealing. After those heat treatments, the ductility of the ribbons was improved, and the coils were slightly looser than before. Therefore, the superconducting coil can be taken off the MgO spools and refit on another spool, or can be enforced by wrapping a protective sheet on the original MgO spool. The processes and properties of the superconducting coils will be reported elsewhere.

4. Conclusions

Metallic precursor ribbons of $Bi_{1.4}Pb_{0.6}Sr_2Cu_3Cu_4$ containing 12–82 vol % Ag were prepared by melt-spinning. Their mechanical properties were investigated as a function of the silver content and the melt-spinning processing parameters. The following conclusions can be drawn based on the present experiments:

1. The metallic precursor ribbons of $Bi_{1.4}Pb_{0.6}Sr_2Cu_3Cu_4$ with 12–82 vol % Ag all possess a fine scale, multiphase crystalline structure. Electron probe

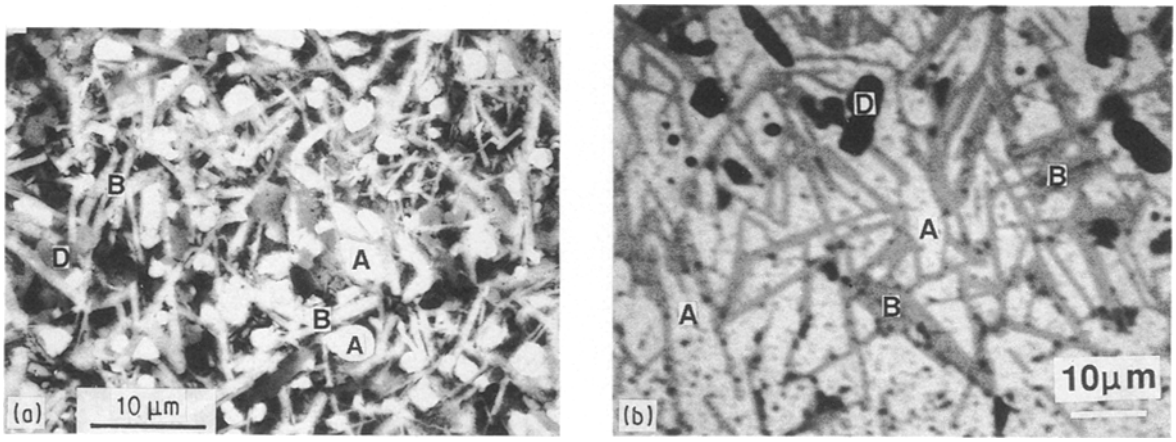

Figure 7 Scanning electron micrographs (backscattered electron images) of typical longitudinal cross section microstructure from (a) $Bi_{1.4}Pb_{0.6}Sr_2Cu_3Cu_4Ag_5$ oxidized at 500 °C in 100% O_2 for 40 h and annealed at 835 °C in 5% O_2 + 95% Ar for 100 h; (b) $Bi_{1.4}Pb_{0.6}Sr_2Cu_3Cu_4Ag_{21}$ oxidized at 600 °C in 100% O_2 for 40 h and annealed at 820 °C in 5% O_2 + 95% Ar for 100 h. A – metallic silver, B – the "2223" superconducting phase and D – $CaCu_2O_3$.

microanalysis showed that the phases and elements are distributed rather homogeneously because of the high cooling rate. The maximum bending strain of the metallic precursor ribbons increased from ~ 0.3 to 1.7% as the silver content increased from 12 to 82 vol % Ag, while the hardness first increased from $H_v = \sim 100$ to ~ 280 as the silver content increased from 12 to ~ 61 vol %, then dropped to $H_v = \sim 200$ as the silver content increased further to 81 vol %.

2. Metallic precursor of $Bi_{1.4}Pb_{0.6}Sr_2Cu_3Cu_4Ag_{21}$ was chosen to investigate the effects of the ejection pressure and wheel speed. The results showed that both the ribbon hardness and the maximum bending strain first increased as the wheel speed increased from 6.3 to 9.5 $m\,s^{-1}$, then decreased as the wheel speed increased further. On the other hand, although the ribbon hardness increased with the decrease of the ejection pressure, the best bending strain of 0.85% was obtained (for this Ag content) when a medium pressure of 69 kPa was applied. It is believed that cooling rate played an important role in the ribbon microstructure and hardness, while the maximum bending strain exhibits a more complicated behaviour, involving the ribbon strength, ductility and perfection.

Acknowledgements

This project is supported by a DOE grant contract No. DE-FGO2-85ER 45179. The authors would like to thank Drs G. Yurek, S. Recca, Ms Y.-L. Xie and Mr. M. Warwick for their assistance and useful discussions.

References

1. G. J. YUREK, J. B. VANDER SANDE, W.-X. WANG, D. A. RUDMAN, Y. ZHANG and M. M. MATTHIESEN, *Metall. Trans.* **18A** (1987) 1813.
2. R. HALDAR, Y. Z. LU and B. C. GIESSEN, *Appl. Phys. Lett.* **51** (1987) 538.
3. G. J. YUREK, J. B. VANDER SANDE and D. A. RUDMAN, *Mat. Res. Soc. Symp. Proc.* **99 MRS** (1988) 619.
4. K. MATSUZAKI, A. INOUE, H. KIMURA, K. AOKI and T. MASUMOTO, *Jpn J. Appl. Phys.* **26** (1987) L1310.
5. WEI GAO, S.-C. LI, D. A. RUDMAN, G. J. YUREK and J. B. VANDER SANDE, *Physica C* **161** (1989) 71.
6. WEI GAO, R. PARRELA, S.-C. LI, D. A. RUDMAN, G. J. YUREK and J. B. VANDER SANDE, *J. Mater. Res.* **5**(11) (1990) 2633.
7. WEI GAO, S.-C. LI, D. A. RUDMAN, G. J. YUREK and J. B. VANDER SANDE, *J. Electrochem. Soc.* **137**(6) (1990) 1951.
8. WEI GAO, S.-C. LI, D. A. RUDMAN, G. J. YUREK and J. B. VANDER SANDE, *Appl. Phys. Lett.* **55**(21) (1989) 2227.
9. P. DADRAS, in "Metals Handbook", 9th edition, Vol. 8, 'Mechanical Testing' (American Society for Metals, Metals Park, Ohio, 1985) p. 118.
10. W. G. MOFFATT, in "The Handbook of Binary Phase Diagrams" (Genium Publishing Corporation, New York, 1986).
11. R. P. ELLIOTT, in "Constitution of Binary Alloys, First Supplement" (McGraw-Hill. New York, 1965).
12. F. A. SHUNK, in "Constitution of Binary Alloys, Second Supplement" (McGraw-Hill, New York, 1969).
13. P. M. HANSEN, in "Constitution of Binary Alloys", 2nd edn with K. Anderko (McGraw-Hill, New York, 1958).
14. H. H. LIEBERMANN and R. L. BYE, Jr, in "Rapidly Solidified Crystalline Alloys", edited by S. K. Das, B. H. Kear and C. M. Adam (Metallurgical Society, 1985) p. 61.
15. S. KAVESH, in "Metallic Glasses", edited by J. J. Gilman and H. J. Leamy (ASM, Metals Park, OH, 1978) p. 36.
16. J. H. VINCENT and H. A. DAVIES, in "Solidification Technology in the Foundry and Casthouse" (The Metal Society, London, 1983) p. 153.
17. L. KATGERMAN (III) and P. J. VAN DEN BRINK, in Proceedings of the 4th International Conference on Rapidly Quenched Metals, edited by T. Masumoto and K. Suzuki (The Japan Institute of Metals, Sendai, Japan, 1982) p. 61.
18. WEI GAO, S.-C. LI, D. A. RUDMAN and J. B. VANDER SANDE, *Physica C.* **167** (1990) 395.

Received 15 March
and accepted 3 December 1990